Inhibition of Apoptosis Reduces Diploidization of Haploid Mouse Embryonic Stem Cells during Differentiation

Wenhao Zhang,[1,4] Yaru Tian,[1,4] Qian Gao,[1,2,4] Xu Li,[1] Yanni Li,[3] Jinxin Zhang,[1] Chunmeng Yao,[1] Yuna Wang,[1] Haoyu Wang,[1] Yiding Zhao,[1] Qian Zhang,[1] Luyuan Li,[1] Yang Yu,[2,*] Yong Fan,[3,*] and Ling Shuai[1,*]

[1]State Key Laboratory of Medicinal Chemical Biology and College of Pharmacy, Nankai University, Tianjin 300350, China
[2]Reproductive Medical Center, Department of Gynecology and Obstetrics, Clinical Stem Cell Research Center, Peking University Third Hospital, Beijing 100191, China
[3]Key Laboratory for Major Obstetric Diseases of Guangdong Province, Key Laboratory of Reproduction and Genetics of Guangdong Higher Education Institutes, The Third Affiliated Hospital of Guangzhou Medical University, Guangzhou 510150, China
[4]Co-first author
*Correspondence: yuyang5012@hotmail.com (Y.Y.), yongfan011@gzhmu.edu.cn (Y.F.), lshuai@nankai.edu.cn (L.S.)
https://doi.org/10.1016/j.stemcr.2020.05.004

SUMMARY

Phenotypes of haploid embryonic stem cells (haESCs) are dominant for recessive traits in mice. However, one major obstacle to their use is self-diploidization in daily culture. Although haESCs maintain haploidy well by deleting *p53*, whether they can sustain haploidy in differentiated status and the mechanism behind it remain unknown. To address this, we induced *p53*-deficient haESCs into multiple differentiated lineages maintain haploid status *in vitro*. Haploid cells also remained in chimeric embryos and teratomas arising from *p53*-null haESCs. Transcriptome analysis revealed that apoptosis genes were downregulated in *p53*-null haESCs compared with that in wild-type haESCs. Finally, we knocked out *p73*, another apoptosis-related gene, and observed stabilization of haploidy in haESCs. These results indicated that the main mechanism of diploidization was apoptosis-related gene-triggered cell death in haploid cell cultures. Thus, we can derive haploid somatic cells by manipulating the apoptosis gene, facilitating genetic screens of lineage-specific development.

INTRODUCTION

Sexually reproductive diploid animals exhibit evolutionary advantages over asexual organisms due to meiosis and the combination of two haploid gametes from different genetic backgrounds (Kondrashov and Crow, 1991; Perrot et al., 1991). Diploid genomes have allelic backups, but this hinders the elucidation of the gene function of recessive traits. Recently developed haploid cell lines, including near-haploid tumor cells (Carette et al., 2009; Gibbons et al., 1991) and haploid embryonic stem cells (haESCs) (Leeb and Wutz, 2011; Sagi et al., 2016), greatly facilitate forward and reverse genetic screening in mammalian species (Li and Shuai, 2017). It is easy to identify not only toxicant-targeting genes (Elling et al., 2011) but also crucial genes regulating critical biological processes (such as differentiation [Leeb et al., 2014] or X chromosome inactivation [Monfort et al., 2015]) through high-throughput screening in haESCs. However, daily cultured haESCs tend to revert to diploid status, and periodic sorting for haploids is necessary, which hampers the application of these cell lines in genetic screening. In addition, haESCs undergo more severe diploidization during differentiation both *in vitro* and *in vivo*, making the derivation of haploid lineage-specific somatic cells very difficult (Shuai and Zhou, 2014). Therefore, spontaneous diploidization of haESCs jeopardizes the exploration of the application of haploid technology in mammalian organ development or disease-related

genetic screening despite their original single-genome status.

Many efforts have been made to clarify the mechanism underlying the diploidization of mammalian haESCs; however, no precise regulatory pathway has yet been found. A previous report showed that the reason for the diploidization of mouse haESCs was a mistake in their cell cycle rather than the fusion of two single haploid cells, as indicated by the coculturing of haESCs with different marker genes (Leeb et al., 2012). Thereafter, chemical compounds inhibiting cell-cycle-related proteins were introduced into the culture medium to reduce diploidization (He et al., 2017; Takahashi et al., 2014), which still did not solve the problem completely. Single-cell dynamic analysis of mitosis in haESCs demonstrated that the metaphase of these cells was significantly longer than that of diploid ESCs (Guo et al., 2017). Thus, delayed mitosis might be the main cause of self-diploidization in haESCs. In this case, time-consuming and complicated fluorescence-activated cell sorting (FACS) was necessary to maintain the haploidy of haESCs. Recent studies showed that knockout of *p53* (Olbrich et al., 2017) or overexpression of *Dnmt3b* (He et al., 2018) could stabilize the haploid genome and slow down self-diploidization. In particular, *p53*-null haESCs could sustain haploid status well both under daily culture and in cells converting to an extraembryonic cell fate (Peng et al., 2019). *p53* is an essential gene related to the cell cycle, DNA damage, and other crucial biological

processes (Aladjem et al., 1998; Cross et al., 1995; Fujiwara et al., 2005). Nevertheless, whether the *p53*-null mutation is beneficial for the maintenance of a haploid status during differentiation is still unknown. The exact mechanism by which *p53*-null reduces self-diploidization is also not clear.

In this study, we deleted *p53* in mouse parthenogenetic haESCs with the CRISPR/Cas9 system and performed differentiation both *in vitro* and *in vivo* to assess whether *p53*-null stabilized haploidy in the somatic stage. The results revealed that by deleting *p53*, haploid somatic cells could be easily obtained from differentiated haESCs. We further analyzed global transcriptome data and found that genes regulating apoptosis were the main reason for diploidization during the differentiation of haESCs.

RESULTS

p53-Null HaESCs Maintain Haploidy Much More Stably Compared with Wild-Type HaESCs under Long-Term Culture

We generated two mouse parthenogenetic haESC lines from chemically activated oocytes according to a previous protocol (Shuai et al., 2014). These haESCs showed a standard mouse ESC morphology (Figure S1A) and grew well with the haploid genome assisted by FACS (Figure S1B). To introduce *p53* mutations in haESCs, we designed two Cas9-mediated *p53*-single guide RNA (sgRNA) vectors to perform electroporation (Figure S1C). Two days after transfection, approximately 58.6% of the analyzed cells were Cas9-GFP-positive (Figure S1D), and these cells were harvested for further culturing. We randomly picked three subclones from the sorted cultures and determined whether they were gene edited. All three subclones (*p53* KO-1, *p53* KO-2, and *p53* KO-3) carried different mutations in the *p53* gene according to DNA sequencing (Figure 1A). The T7EN1 cleavage assay results also confirmed this (Figure 1B). To assess whether the P53 protein was lost, we performed western blotting in *p53* KO-1, *p53* KO-2, *p53* KO-3, wild-type (WT) haESCs, and WT diploid ESCs (WT-diESCs). The results demonstrated that P53 was absent in all three *p53*-KO haESC lines (Figure 1C).

To determine whether *p53* mutation affects the pluripotency of haESCs, we examined specific markers and alkaline phosphatase activity in *p53*-KO haESCs. Positivity was observed not only for pluripotency markers (OCT4, NANOG, and SSEA-1) but also for alkaline phosphatase in *p53*-KO haESCs (Figures S1E and S1F). Karyotype analysis showed that most chromosome spreads of *p53*-KO haESCs contained 20 chromosomes (Figure S1G). Next, we analyzed pluripotent genes and *p53*-related genes in *p53*-KO haESCs by real-time PCR with WT-haESCs as a control. The expression levels of pluripotent markers (*Oct4* and

Nanog) and *Cyclin B* did not change significantly in *p53*-KO haESCs compared with WT-haESCs. However, expression of *p53* and *p21* decreased, meanwhile *Cdk2* and *MAPK11* increased significantly in all three *p53*-KO haESC lines (Figure 1D). This result indicated that *p53* mutations did not affect pluripotency but do affect *p53*-related genes, including some cell-cycle genes. Since *p53* deletion increased haploidy maintenance in the ESC stage, as previously described, we tested whether *p53*-KO haESCs exhibited advantages in haploidy maintenance in daily culture without sorting for 3 weeks. There was still a high percentage of haploid cells remaining in the 1n peak (G_0/G_1 phase) of *p53*-KO haESCs (*p53* KO-1, 21.4%; *p53* KO-2, 20.9%; *p53* KO-3, 20.2%), whereas the percentage of the 1n peak (G_0/G_1 phase of haploid cells) in WT-haESCs decreased to 2.4% (Figure 1E). Here, we chose *p53* KO-1 (the most stable) for subsequent experiments. We designed *p53* overexpression (*p53* OE) vectors (Figure S1H) and transferred them into *p53* KO-1 cells having a high proportion of haploids, with an empty vector as control. After transfection, transfected cells expressing exogenous GFP (a GFP cassette was included in the *p53* OE vector or empty vector) were enriched for GFP and haploidy double-positive cells by FACS (Figures 1F and 1G). Real-time PCR result revealed that *p53* OE-haESCs (*p53* KO-1-*p53* OE) had re-expressed *p53* gene compared with WT-haESCs, *p53* KO-1, and *p53* KO-1-vector (Figure 1H). Western blotting analysis further confirmed this result (Figure S1I). Thereafter, we checked the haploidy-maintaining ability among *p53* KO-1, *p53* KO-1-vector, WT-haESCs, and *p53* KO-1-*p53* OE cells without sorting for 10 days (all the samples started as 100% of haploid cells). DNA-content analysis demonstrated that only *p53* KO-1 and *p53* KO-1-vector were able to maintain haploidy stably in this period, whereas *p53* KO-1-*p53* OE and WT-haESCs diploidized to some degree (Figure 1I). The rescue of *p53* expression in *p53*-KO haESCs made them unable to sustain the phenotype of stable haploidy any longer, which proved that *p53* was the main trigger of the diploidization phenomenon. As *Cdk2* and *MAPK11* (two important cell-cycle genes) were upregulated in *p53*-KO haESCs according to the above qPCR analysis, we conducted overexpression (OE) of *Cdk2* and *MAPK11* separately in WT-haESCs to address whether either of the two genes would affect the process of diploidization. Although the OE-haESCs showed upregulation of *Cdk2* and *MAPK11* independently (Figures S1J and S1K), neither of them obtained an advantage in maintaining haploidy like *p53*-KO in long-term cell culture (Figure S1L).

p53-Null HaESCs Differentiate Reliably with a Haploid Genome *In Vitro*

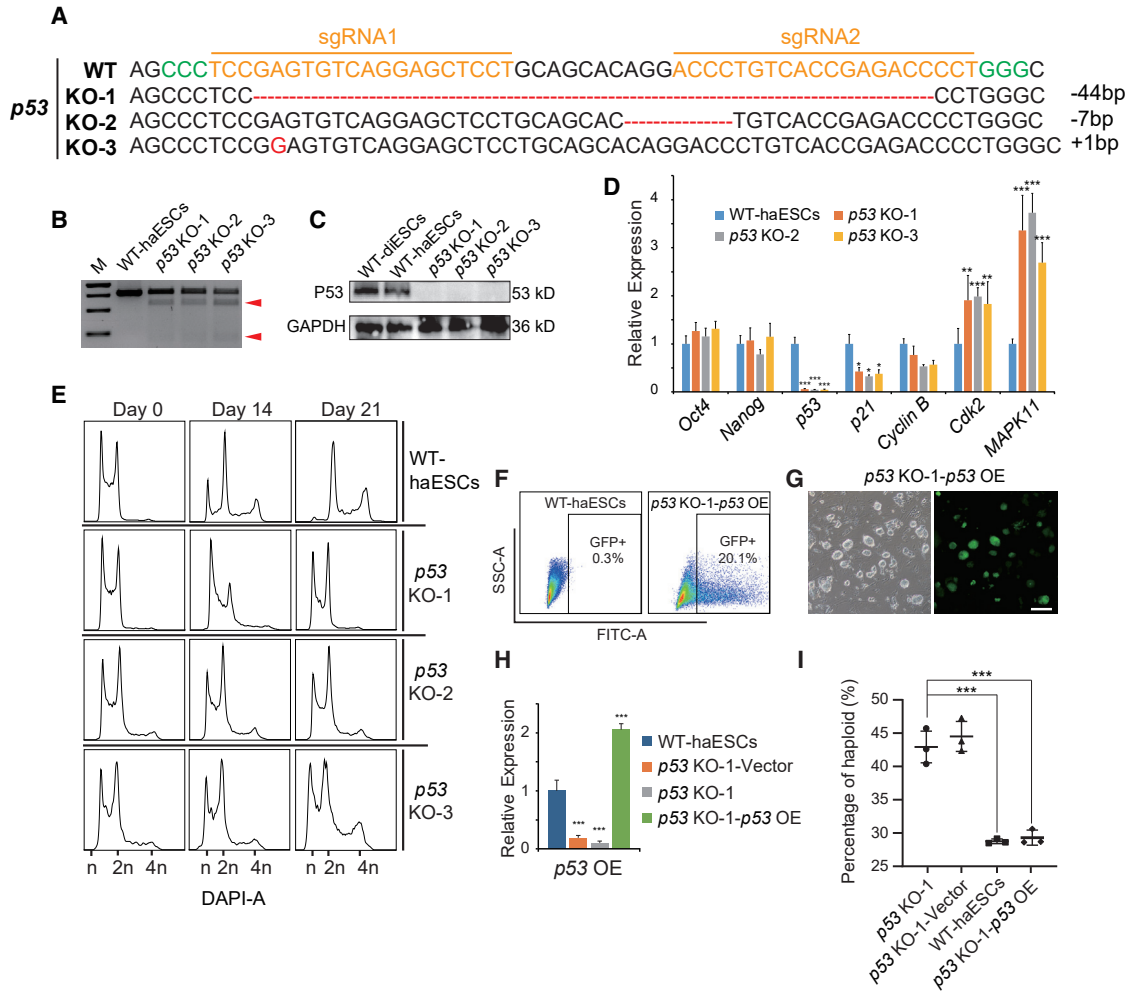To examine the haploid-maintaining ability of *p53*-KO haESCs during differentiation *in vitro*, we performed

Figure 1. *p53* Deletion in haESC and DNA Analysis during Proliferation

(A). *p53*-deleted genotypes in subclones *p53* KO-1, *p53* KO-2, and *p53* KO-3.

(B) T7ENI cleavage analysis of the *p53*-KO lines *p53* KO-1, *p53* KO-2, and *p53* KO-3. Cleaved products (red arrowheads) indicate the presence of mutations.

(C) Western blotting to detect P53 in WT-diESCs, WT-haESCs, *p53* KO-1, *p53* KO-2, and *p53* KO-3 cells. GAPDH was used as a loading control.

(D) Expression levels of pluripotent, *p53*-related, and cell-cycle-related genes (*Oct4, Nanog, p53, p21, CyclinB, Cdk2,* and *MAPK11*) in WT-haESCs, *p53* KO-1, *p53* KO-2, and *p53* KO-3 cells determined by qPCR (n = 3 independent experiments). Data presented as mean ± SEM. t test: *p < 0.05, **p < 0.01, ***p < 0.001.

(E) DNA content analysis of *p53*-KO haESCs during culture on day 0, day 14, and day 21 without sorting, with WT-haESCs as a control. The percentages of the 1n (G_0/G_1) peak in WT-haESCs were 27.4%, 9.33%, and 2.4%, respectively; in *p53* KO-1 cells, 23.5%, 22.8%, and 21.4%, respectively; in *p53* KO-2 cells, 23.6%, 21.1%, and 20.9%, respectively; in *p53* KO-3 cells, 23.7%, 21.5%, and 20.2%, respectively.

(F) Percentage of GFP+ cells in *p53* KO-1-*p53* OE cells after transfection. WT-haESCs without transfection were used as a negative control.

(G) Bright-field (BF) and FITC images of *p53* KO-1-*p53* OE cells, Scale bar, 100 μm.

(H) Expression levels of *p53* in WT-haESCs, *p53* KO-1-Vector, *p53* KO-1, and *p53* KO-1-*p53* OE cells determined by qPCR (n = 3 independent experiments). Data presented as mean ± SEM. t test: ***p < 0.001.

(I) Percentages of haploids in *p53* KO-1, *p53* KO-1-Vector, WT-haESCs, and *p53* KO-1-*p53* OE cells 10 days after sorting. Nearly 44% of sorted cells remained in haploidy in *p53* KO-1 and *p53* KO-1-Vector group, whereas WT-haESCs and *p53* KO-1-*p53* OE exhibited only 29% staying as haploid cells (n = 3 independent experiments). Data presented as mean ± SEM. t test: ***p < 0.001.
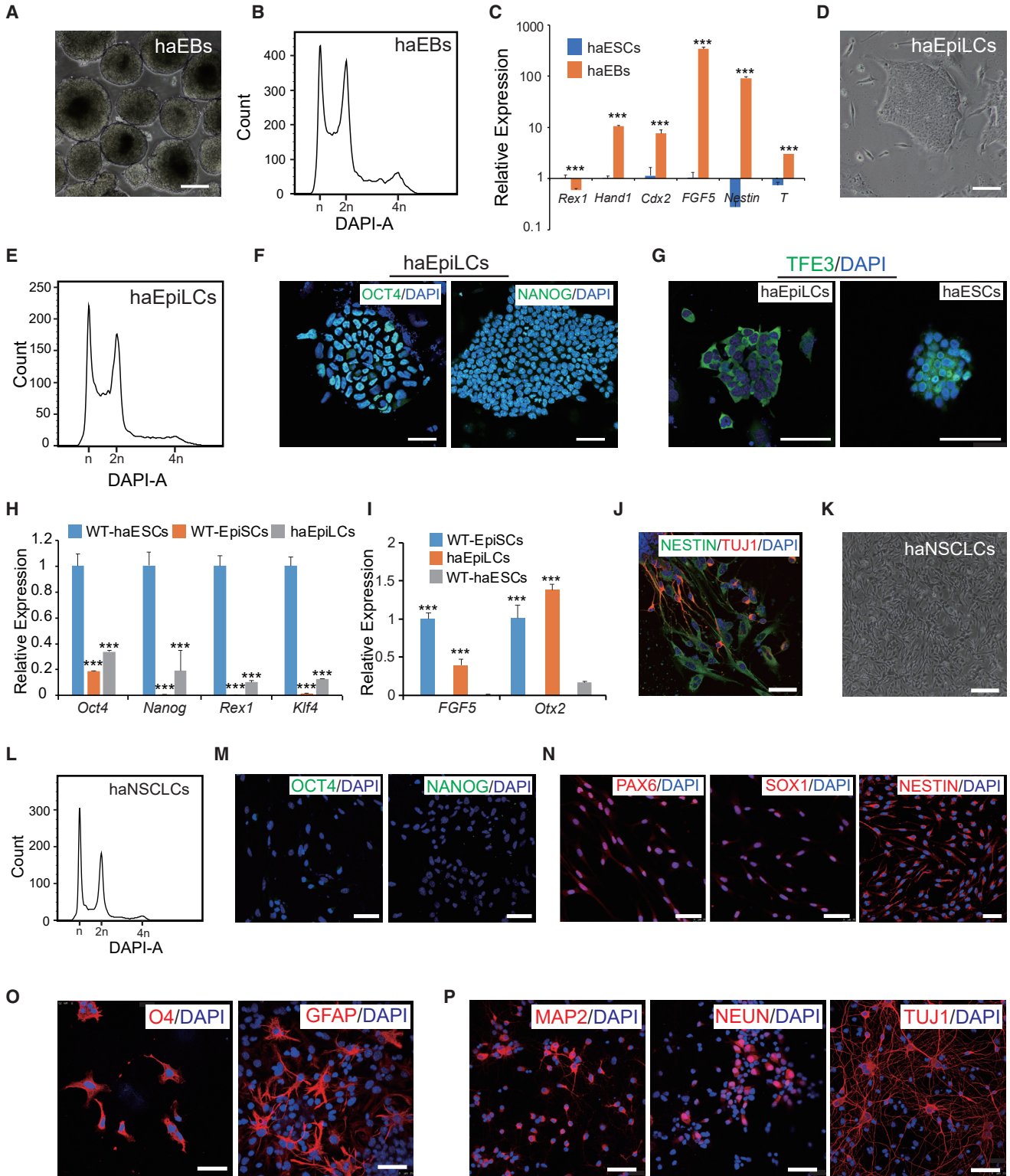
See also Figure S1 and Table S4.

Figure 2. *In Vitro* Differentiation of *p53*-KO haESCs

(A) Morphology of 7-day haEBs derived from *p53* KO-1 cells. Scale bar, 100 μm.

(B) DNA-content analysis of 7-day haEBs derived from *p53* KO-1 cells. The percentage of the 1n (G_0/G_1) peak in haEBs was 21.7%.

(legend continued on next page)

differentiation of *p53*-KO haESCs at different stages. Standard embryoid bodies (EBs) formed (Figure 2A), and 29.7% of haploid cells (at G_0/G_1 phase) were observed in 7-day EBs from *p53*-KO haESCs (Figure 2B). The expression levels of pluripotency genes and specific genes of the three germ layers showed that the haploid EBs had differentiated beyond the ESC stage (Figure 2C). Although WT parthenogenetic haESCs were not able to remain in the epiblast stem cell-like cell (EpiLC) stage with a haploid genome (Leeb et al., 2012), *p53*-KO haESCs differentiated into haploid EpiLCs (haEpiLCs) quite easily and stably sustained haploidy (Figures 2D and 2E). The primed state haEpiLCs expressed pluripotent markers such as OCT4 and NANOG (Figure 2F). Besides, naive-primed distinguishing marker TFE3 (Betschinger et al., 2013) was located in the cytoplasm of haEpiLCs (Figure 2G), demonstrating that *p53*-KO haEpiLCs could remain in the epiblast stage with a single genome in the presence of basic fibroblast growth factor (bFGF) and activin A. The expression levels of specific genes further proved that these haploid cultures expressed primed stage genes (*FGF5* and O*tx2*), rather than naive genes (*Rex1* and *Klf4*), with WT-haESCs and WT epiblast stem cells (WT-EpiSCs) as controls (Figures 2H and 2I). To assess differentiation potentials of haEpiLCs, we induced neural differentiation according to a previous protocol (Ying et al., 2003). Around 7–10 days post differentiation, NESTIN- and TUJ1-positive cells were observed in the cell cultures (Figure 2J), indicating that haEpiLCs possessed pluripotency to differentiate to the next stage.

Although haploid neural progenitor cells (Elling et al., 2011) and haploid neurons (Xu et al., 2017) could be detected transiently, it is very difficult to obtain stable haploid neural stem cell-like cells (NSCLCs) by traditional methods. Whether *p53*-KO haESCs could differentiate into somatic stages and maintain haploidy required further investigation. We introduced endogenous NSCLC-specific *Pax6*-GFP into *p53*-KO haESCs according to our previous protocol (Li et al., 2018b). We performed neural differentiation of *p53* KO-1 cells and found that there were 22.3% of *Pax6*-GFP-positive cells among the differentiated derivatives (Figure S2A). Interestingly, there were 6.2% of *Pax6*-GFP-positive cells in the 1n peak, whereas there were 27.8% of *Pax6*-GFP-negative cells in the 1n peak (Figure S2B). These findings demonstrated that diploidization occurred but was slowed down during the differentiation of *p53*-KO haESCs. Haploid and *Pax6*-GFP double-positive cells were enriched by FACS to derive haNSCLCs for further culture. The haNSCLCs showed the standard neural stem cell morphology when cultured under adherent conditions (Figure 2K), presenting the ability to aggregate into neural spheres (Figure S2C). DNA analysis revealed that the haNSCLCs could stably maintain haploidy during proliferation (Figure 2L). Next, we examined pluripotent and neural stem cell-specific markers in haNSCLCs by immunostaining. Pluripotent markers (OCT4 and NANOG) were absent in haNSCLCs (Figure 2M). Positivity for PAX6, SOX1, and NESTIN was observed in adherent haNSCLCs (Figure 2N) and their neural spheres (Figure S2D). To assess the differentiation potential of haNSCLCs, we performed neural lineage specification. The results showed that glial cells (O4 and glial fibrillary acidic protein [GFAP] positive) and multiple neurons (MAP2, NEUN, and TUJ1 positive) could be generated from haNSCLCs (Figures 2O and 2P). In another parallel experiment, we analyzed DNA contents of glial mixture and neuronal mixture independently. There was 2.0% of glial mixture and 4.5% of neuronal

(C) Expression levels of pluripotency and differentiation genes (*Rex1*, *Hand1*, *Cdx2*, *Fgf5*, *Nestin*, and *T*) in haEBs and haESCs determined by qPCR (n = 3 independent experiments). Data presented as mean ± SEM. t test: ***p < 0.001.

(D) Morphology of haEpiLCs derived from *p53* KO-1 cells. Scale bar, 100 μm.

(E) DNA-content analysis of haEpiLCs derived from *p53* KO-1 cells. The percentage of the 1n (G_0/G_1) peak in haEpiLCs was 21.8%.

(F) Immunofluorescence of OCT4 and NANOG in haEpiLCs derived from *p53* KO-1 cells. DNA was stained with DAPI. Scale bar, 50 μm.

(G) Immunofluorescence of TFE3 in haEpiLCs derived from *p53* KO-1 cells and haESCs. DNA was stained with DAPI. Scale bar, 50 μm.

(H) Expression levels of pluripotency genes (*Oct4*, *Nanog*, *Rex1*, and *Klf4*) in WT-haESCs, WT-EpiSCs, and haEpiLCs determined by qPCR (n = 3 independent experiments). Data presented as mean ± SEM. t test: ***p < 0.001.

(I) Expression levels of EpiSC-specific marker genes (*Fgf5* and *Otx2*) in WT-haESCs, WT-EpiSCs and haEpiLCs determined by qPCR (n = 3 independent experiments). Data presented as mean ± SEM. t test: ***p < 0.001.

(J) Immunostaining of NESTIN and TUJ1 in 10-day differentiation cell cultures of haEpiLCs. Scale bar, 50 μm.

(K) Morphology of haNSCLCs derived from *p53* KO-1 cells. Scale bar, 100 μm.

(L) DNA-content analysis of haNSCLCs derived from *p53* KO-1 cells. The percentage of the 1n (G_0/G_1) peak in haNSCLCs was 28.5%.

(M) Immunofluorescence of OCT4 and NANOG in haNSCLCs. DNA was stained with DAPI. Scale bar, 50 μm.

(N) Immunofluorescence of neural stem cell-specific markers in haNSCLCs, PAX6, SOX1, and NESTIN. DNA was stained with DAPI. Scale bar, 50 μm.

(O) Immunostaining of oligodendrocytes (O4) and astrocytes (GFAP) derived from *p53* KO-1. Scale bar, 50 μm.

(P) Immunostaining of neuronal specific markers (MAP2, NEUN, and TUJ1) in neurons derived from *p53* KO-1. Scale bar, 50 μm.
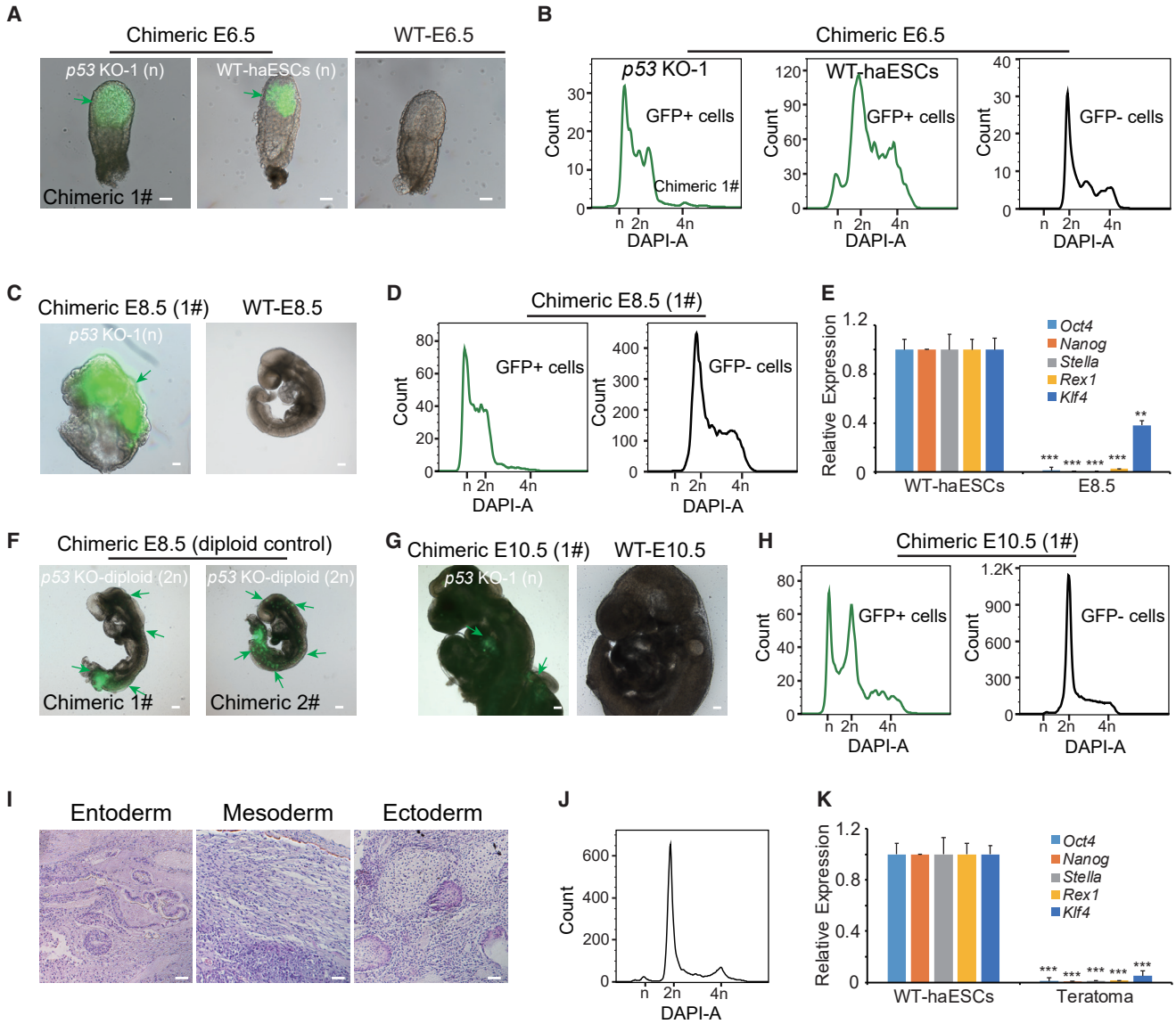
See also Figure S2 and Table S4.

Figure 3. *In Vivo* Analysis of *p53*-KO haESCs

(A) Morphology of chimeric embryos at E6.5 derived from GFP-labeling WT-haESCs and *p53* KO-1 cells. Scale bar, 100 μm. WT-E6.5 embryo was used as a control.

(B) DNA-content analysis of GFP$^+$ cells and GFP$^-$ cells in chimeric E6.5 embryos derived from GFP-labeling WT-haESCs and *p53* KO-1 cells. The percentages of the 1n (G$_0$/G$_1$) peak in GFP$^+$ cells from *p53* KO-1 E6.5 and WT-haESCs E6.5 were 28.5% and 4.7%, respectively.

(C) Morphology of chimeric embryo at E8.5 derived from GFP-labeling *p53* KO-1 cells. WT-E8.5 embryo was used as a control.

(D) DNA-content analysis of GFP$^+$ cells and GFP$^-$ cells in chimeric E8.5 embryo derived from GFP-labeling *p53* KO-1 cells. The percentage of the 1n (G$_0$/G$_1$) peak from *p53* KO-1 chimeric E8.5 GFP$^+$ cells was 25.3%.

(E) Expression levels of pluripotency genes (*Oct4*, *Nanog*, *Stella*, *Rex1*, and *Klf4*) in chimeric E8.5 haploid cells from GFP$^+$ cells, with WT-haESCs as a loading control (n = 3 independent experiments). Data presented as mean ± SEM. t test: **p < 0.01, ***p < 0.001.

(F) Morphology of chimeric embryos at E8.5 derived from GFP-labeling *p53* KO-diploid cells.

(G) Morphology of chimeric embryos at E10.5 derived from GFP-labeling *p53* KO-1 cells. WT E10.5 was used as a control.

(H) DNA-content analysis of GFP$^+$ cells and GFP$^-$ cells in chimeric E10.5 embryo derived from GFP-labeling *p53* KO-1 cells. The percentage of the 1n (G$_0$/G$_1$) peak from *p53* KO-1 chimeric E10.5 GFP$^+$ cells was 21.4%.

(I) Teratoma formed from *p53* KO haESCs was identified by H&E staining. Scale bar, 100 μm. The tissues shown were gut epithelium (endoderm), muscle (mesoderm), and neural tissue (ectoderm).

(J) DNA-content analysis of teratoma. The percentage of the 1n (G$_0$/G$_1$) peak from all the tissue was 3.1%.

(legend continued on next page)

mixture remaining in the 1n peak, respectively (Figures S2E and S2F), indicating that haNSCLCs possessed multipotency for neural lineages with a haploid genome.

Haploid Cells Can Contribute to Chimeric Fetuses and Teratomas upon *p53* Knockout

The finding that *p53*-KO haESCs showed excellent haploidy maintenance during differentiation *in vitro* led to the further investigation of whether they presented the same advantages during differentiation *in vivo*. We microinjected GFP-labeling *p53*-KO haESCs into blastocysts to construct chimeric embryos. The reconstructed embryos were transferred to the oviducts of 0.5 days post coitum (dpc) pseudopregnant mice. Chimeric embryonic day 6.5 (E6.5) embryos from GFP-labeling *p53*-KO haESCs and GFP-labeling WT-haESCs were obtained (Figures 3A and S3A). Around 17.2% cells of chimeric E6.5 1# embryo and 55.5% cells of chimeric E6.5 2# embryo generated from *p53*-KO haESCs microinjection were GFP-positive cells (Table S1). The haploid cells in the 1n peak of *p53*-KO haESCs-chimeric E6.5 embryos (*p53* KO-1, chimeric 1#, 28.5%; *p53* KO-2, chimeric 2#, 24.5%) were much higher than that in WT-haESCs-chimeric E6.5 embryo (WT-haESCs-chimeric, 4.7%) (Figures 3B and S3B; Table S1), demonstrating that *p53*-KO haESCs could contribute to an epiblast stage with a high proportion of haploid status. For chimeric E8.5 embryos, 12.4% cells of 1# embryo and 37.6% cells of 2# embryo from *p53*-KO haESCs microinjection were GFP-positive cells (Table S1). However, chimeric E8.5 embryos from *p53*-KO haESCs were abnormal (Figures 3C and S3C), possibly due to the high contribution of haploid cells (a haploid genome might not support full development) or deficiency of *p53*, with approximately 25% of these cells (*p53* KO-1, chimeric 1#, 25.3%; *p53* KO-2, chimeric 2#, 24.3%) remaining in the 1n peak (Figures 3D and S3D). To address the identity of these haploid cells from E8.5 embryos, we harvested them by FACS and performed qPCR analysis. Compared with WT-haESCs, the sorted haploid cells barely expressed any of the pluripotent markers (*Oct4*, *Nanog*, *Stella*, *Rex1*, and *Klf4*), demonstrating that they were indeed differentiated cells (Figure 3E). Thus, *p53*-KO haESCs could differentiate into a somite stage without diploidization. To investigate the effect of *p53* deletion on development, we microinjected GFP-labeling *p53*-KO diploid ESCs into blastocysts as a parallel experiment. Interestingly, chimeric E8.5 embryos from *p53*-KO diploid ESCs were normal (Figure 3F), with GFP cells (24.9% in 1# and 40.3% in 2#) contributing to the chimeric E8.5 embryos (Table S1). Furthermore, abnormal chimeric E10.5 embryos were also able to be obtained (Figures 3G and S3E). The percentages of GFP cells in chimeric E10.5 1# and 2# embryos from *p53*-KO haESCs microinjection were 1.6% and 3.3%, respectively (Table S1). According to DNA analysis, there were still around 22% of haploid cells in 1n peak (*p53* KO-1, chimeric 1#, 21.4%; *p53* KO-2, chimeric 2#, 22.3%) from E10.5 GFP-positive cells (Figures 3H and S3F), indicating that *p53*-KO haESCs could further differentiate in a haploid genome with limited development potentials.

To check the pluripotency of *p53*-KO haESCs to form the three germ layers, we injected approximately 1×10^7 *p53* KO-1 cells under the skin of severe combined immunodeficiency (SCID) mice. Three weeks later, a standard teratoma formed (Figures S3G and S3H) and was divided into two parts. Histological analysis was performed on one part, and DNA-content analysis was performed on the other. Gut epithelium, muscle, and neural tube tissues, representing the three germ layers, were observed by H&E staining (Figure 3I). According to the DNA-content analysis, 3.1% haploid cells (1n peak) still existed in the 3-week teratoma, demonstrating that the *p53*-KO haESCs show a powerful ability to maintain haploidy *in vivo* (Figure 3J). The haploid cells from teratoma were also sorted by FACS and checked by qPCR. The result showed that the haploid cells in teratoma did not express the pluripotent marker genes (*Oct4*, *Nanog*, *Stella*, *Rex1*, and *Klf4*), indicating that they had entered a differentiated state instead of a pluripotent state (Figure 3K).

Transcriptome Analysis of *p53*-KO HaESCs

To determine why *p53*-KO haESCs show great advantages in haploidy maintenance, we compared the transcriptomes between *p53*-KO haESCs and WT-haESCs by RNA-sequencing (RNA-seq) analysis. The results revealed a very high correlation ($R^2 = 0.9947$) between *p53*-KO haESCs (*p53* KO-1, *p53* KO-2, and *p53* KO-3) and WT-haESCs (three independent WT-haESC lines) (Figure 4A). According to comprehensive summaries with all expression data (Tables S2 and S3), there were 2,785 differentially expressed genes ($p < 0.01$, fold change >2) between *p53*-KO haESCs and WT-haESCs, which were further analyzed to elucidate the reason of haploidy stabilization. Hierarchical clustering (heatmap) showed the top 50 differentially expressed genes between *p53*-KO haESCs and WT-haESCs, considering a fold change of 2.0 and $p < 0.05$ (Figure S4A and Table S2). These differentially expressed genes were mainly related to the extracellular matrix and basic development according to gene ontology (GO) analysis (Figures S4B and S4C).

(K) Expression levels of pluripotent genes (*Oct4*, *Nanog*, *Stella*, *Rex1*, and *Klf4*) in the 1n cells sorted from teratoma determined by qPCR, with WT-haESCs as a loading control (n = 3 independent experiments). Data presented as mean ± SEM. t test: ***p < 0.001. See also Figure S2; Tables S1 and S4.

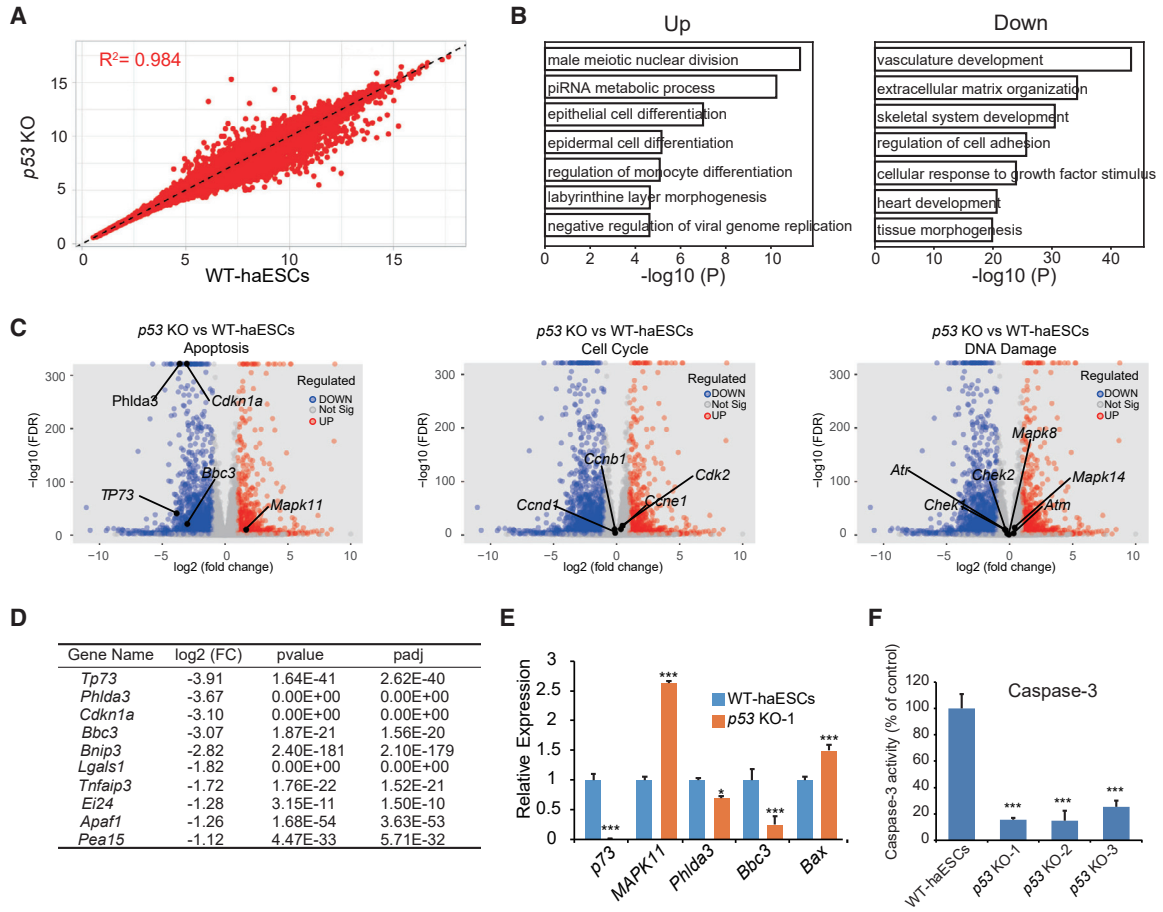**Figure 4. Transcriptome of *p53*-KO haESCs**

(A) Scatterplot of log$_2$ transformed average gene expression profiles. Global gene expression of three *p53*-KO haESCs (*p53* KO-1, *p53* KO-2, and *p53* KO-3) and three WT-haESC lines (WT-haESCs-1, WT-haESCs-2, and WT-haESCs-3) were analyzed by scatterplot (R^2 is the Pearson correlation coefficient).

(B) Enriched gene ontologies of upregulated and downregulated genes in *p53*-KO haESCs.

(C) Volcano plot depicting the differential expression analysis between WT-haESCs and *p53*-KO haESCs. The higher location of the point of the gene, the more significant the difference. Highlighted points indicate genes correlated with apoptosis, cell cycle, and DNA damage, respectively, considering a fold change of 2.0 and p < 0.05.

(D) Top ten genes correlated with apoptosis in the differential expression analysis between WT-haESCs and *p53* KO haESCs.

(E) Expression levels of apoptosis-related genes (*p73*, *Phlda3*, *Bbc3*, and *Bax*) and a proliferation-related gene (*MAPK11*) in WT-haESCs and *p53*-KO haESCs determined by qPCR (n = 3 independent experiments). Data presented as mean ± SEM. t test: *p < 0.05, ***p < 0.001.

(F) Caspase-3 activity of *p53* KO-1, *p53* KO-2, and *p53* KO-3 cells, with WT-haESCs as a control (n = 3 independent experiments). Data presented as mean ± SEM. t test: ***p < 0.001.

See also Figure S4 and Tables S2, S3, and S4.

GO analysis data further indicated that most of the upregulated genes were correlated with male meiotic nuclear division, Piwi-interacting RNA metabolic process, and other biological processes, whereas the downregulated genes were related to vasculature development and extracellular matrix organization (Figure 4B). Since *p53* is a very important gene involved in multiple biological processes, including DNA-damage repair, cell-cycle arrest, and apoptosis (Hafner et al., 2019), we analyzed the expression

of specific genes involved in these processes between *p53*-KO haESCs and WT-haESCs in volcano plots of p values (−log$_{10}$ scale) versus fold changes (log$_2$ scale). Interestingly, there were several differentially expressed genes related to apoptosis identified between the two groups (Figure 4C). However, we did not observe distinctly expressed genes related to the cell cycle or DNA damage in the RNA-seq data (Figure 4C). As we also found that the *p53*-KO haESCs showed better survival ability during differentiation
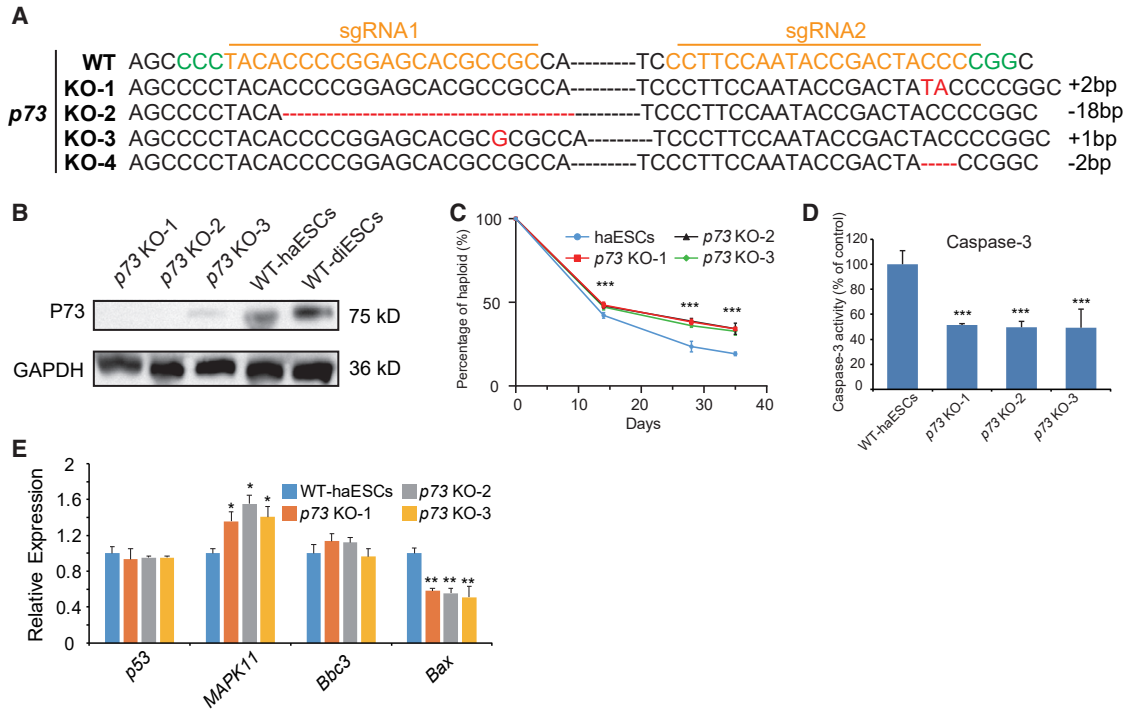
Figure 5. *p73* Is a Major Target of *p53*-Regulating Diploidization

(A) *p73*-deleted genotypes in haESCs by DNA sequencing.

(B) Western blot to detect P73 in *p73* KO-1 cells, *p73* KO-2 cells, *p73* KO-1 cells, WT-haESCs, and WT-diESCs. GAPDH was used as a loading control.

(C) Progression of the percentage of haploid cells in the *p73*-KO haESCs and WT-haESCs for 14 days, 28 days, and 35 days after sorting (n = 3 independent experiments). Data presented as mean ± SEM. t test: ***p < 0.001.

(D) Caspase-3 activity of *p73* KO-1, *p73* KO-2, and *p73* KO-3 cells, with WT-haESCs as a control (n = 3 independent experiments). Data presented as mean ± SEM. t test: ***p < 0.001.

(E) Expression levels of apoptosis-related genes (*p53*, *Bbc3*, and *Bax*) and proliferation-related gene *MAPK11* in *p73* KO-1, *p73* KO-2, and *p73* KO-3 haESCs determined by qPCR, with WT-haESCs as a control (n = 3 independent experiments). Data presented as mean ± SEM. t test: *p < 0.05, **p < 0.01.

See also Figure S5 and Table S4.

compared with WT-haESCs *in vitro* (data not shown), we assessed carefully the differentially expressed genes correlated with apoptosis. *TP73* (*p73*, also known as *Trp73*), *Phlda3*, *Cdkn1a*, and *Bbc3* (downstream target genes of *p53*) were significantly downregulated in *p53*-KO haESCs (Figure 4D) and were listed as the top four downregulated genes in *p53*-KO haESCs related to apoptosis. We further detected the expression levels of some target genes of *p53* related to apoptosis by qPCR and found that only *p73* and *Bbc3* were significantly downregulated (Figure 4E).

To address whether apoptosis was the main reason for the diploidization of haESCs, we assessed the survival rate of *p53*-KO haESCs 24 h after sorting for haploids compared with WT-haESCs. Nearly 70.5% of the sorted cells survived and expanded in the *p53*-KO group, whereas in the control group this percentage was only 52.9% (Figure S4D). As caspase-3 is a key molecule in the process of

apoptosis (Song et al., 2015), we measured the caspase-3 activity between *p53*-KO haESCs and WT-haESCs after sorting. The caspase-3 activities in *p53* KO-1, *p53* KO-2, and *p53* KO-3 were significantly decreased compared with that in WT-haESCs (Figure 4F). In summary, apoptosis of *p53*-KO haESCs was reduced in daily culture and FACS processes.

p73 Is a Major Target of p53-Regulating Diploidization

To find out more about apoptosis-related gene-regulating diploidization, we designed *p73* and *Bbc3* knockout vectors (Figures S5A and S5B) and transfected them separately into WT-haESCs to introduce gene editing. Among the 60 randomly picked subclones of the *p73*-edited group, 25 subclones maintained haploidy (Figure S5C). We sequenced 11 subclones with high percentages of haploid cells and found that four of them were *p73*-KO cells

(Figure 5A). To assess whether the P73 protein was lost, we performed western blotting in *p73* KO-1, *p73* KO-2, *p73* KO-3, WT-haESCs, and diploid ESCs. The results demonstrated that P73 was absent in three *p73*-KO haESC lines (Figure 5B). However, in the *Bbc3*-edited group, 18 out of 60 randomly selected subclones exhibited haploid cells, 9 of which showed a high percentage of haploids, which were sequenced and did not contain a *Bbc3* mutation (Figure S5C). We randomly checked two diploidized subclones by sequencing and found *Bbc*3 mutations (Figure S5D). DNA-content analysis again confirmed that the *Bbc3* mutant subclones were diploid, without any haploid cells (Figure S5E). Notably, this result indicated that *p73* alone was the key regulator of diploidization, rather than *Bbc3*. We further assessed whether *p73*-KO haESCs also showed advantages in haploidy maintenance similar to those of *p53*-KO haESCs. The results demonstrated that *p73*-KO haESCs exhibited better proliferation ability after sorting (Figure S5F) and a lower rate of diploidization during long-term culture (Figure 5C) compared with WT-haESCs. The caspase-3 activity in *p73* KO-1, *p73* KO-2, and *p73* KO-3 was much lower than that in WT-haESCs, suggesting that apoptosis could be inhibited by *p73*-KO (Figure 5D). Next, we examined the expression of *p53*-targeted genes related to apoptosis in *p73*-KO haESCs (*p73* KO-1, *p73* KO-2 and *p73* KO-3) and WT-haESCs and did not find any significant differences in the downstream gene (Figure 5E). This result indicated that *p73* played a crucial role in affecting diploidization without interacting with its upstream genes, including *p53*.

DISCUSSION

Haploidy in lower organisms, including yeast, is fairly stable, which makes haploid individuals a powerful tool for genetic engineering (de Godoy et al., 2008). Medaka fish haESCs also show durable haploidy in both undifferentiated and differentiated statuses, despite being vertebrate species (Yi et al., 2009). However, mammalian haESCs tend to revert to diploidy under daily culture or differentiation, making complicated and frequent sorting of haploids necessary. Although haNSCLCs have been obtained by an optimized epiblast-based method (Shuai et al., 2015) or by introducing a ROCK inhibitor (Y27632) into the culture medium (He et al., 2017), these cells are not easy to handle, and the underlying mechanisms require further investigation. Our findings provide a simple strategy for deriving multiple haploid somatic cells by knocking out a single gene (*p53*-KO or *p73*-KO). We find that reduced apoptosis may be a major reason why *p53*-KO haESCs stably maintain haploidy. Additionally, knockout of *p73*, a target of *p53*, can also stabilize haploidy in haESCs.

Although *p53* or *p73* deficiency can promote haploidy maintenance in mouse haESCs, whether this phenomenon is applicable to other species remains unknown. Previous studies reported that primate haESCs maintain haploidy more stably than rodent haESCs (Sagi et al., 2016; Yang et al., 2013), and whether the mechanisms involved correlate with *p53* or *p73* warrants further investigation. Another study showed that although rhesus monkey haESCs maintained haploidy well in the ESC state, they underwent severe diploidization during differentiation for reasons related to apoptosis (Wang et al., 2018). Therefore, apoptosis may be the major cause of the diploidization of mammalian haploid cells. Generally, both haESCs and haploid somatic cells do not exhibit growth properties equivalent to those of their diploid counterparts (Olbrich et al., 2017). Our data revealed that *p53*-KO or *p73*-KO haESCs survived better after FACS (Figure S4D) and regained their proliferative ability faster (Figure S5F) than WT-haESCs. Previous studies have indicated that some haESCs experience cell-cycle errors such as mitosis escape, resulting in diploidization (Guo et al., 2017; He et al., 2017). According to our RNA-seq data, however, *p53*-KO haESCs did not show significant changes in the expression of cell-cycle-related genes (Figure 4C). We propose that the stabilization of haploidy in *p53*-KO haESCs depended on a reduction in apoptosis instead of regulation of the cell cycle. Nevertheless, both *p53* and *p73* are essential genes involved in many pathways, including key cell-cycle checkpoints (Melino et al., 2002; Stiewe, 2007). The exact mechanism by which *p53*-KO or *p73*-KO haESCs avoid mitosis escape has not yet been clarified.

Due to diploidization, complicated and time-consuming FACS purification is necessary for haploidy maintenance. Non-staining sorting methods have been introduced to enrich haploids (Freimann and Wutz, 2017; Qu et al., 2018), but their efficiency cannot be guaranteed. In our study, *p53*-KO or *p73*-KO haESCs could maintain haploidy without sorting for at least 3 weeks, which facilitates the expansion of large-scale haploid cell cultures rapidly for high-throughput genetic screening. However, previous reports demonstrated that *p53*-deficiency diploid ESCs showed limited pluripotency (Li et al., 2018a; Lin et al., 2005). In our study, *p53*-KO haESCs also showed nearly 2,800 differentially expressed genes from WT-haESCs at global transcriptome level. This indicated that there might be potential restriction of *p53*-KO haESCs in differentiation, which needs further investigation. Nevertheless, *p53*-KO haESCs could contribute to chimeras (up to E10.5) and teratomas in haploid status, which would mean that haploid somatic cells could be derived in a rigorous way *in vivo*, thus expanding the application of such a haploid system for lineage-specific genetic screening.

EXPERIMENTAL PROCEDURES

Transfection

To obtain *p53*-KO haESC lines, we electroporated approximately 4×10^6 WT-haESCs with PX461-sgRNA1 (3 μg) and PX461-sgRNA2 (3 μg), using a Neon (Invitrogen) electroporator at 1,400 V for 10 ms with three pulses. GFP-positive cells were sorted by FACS 2 days post electroporation. For the overexpression of *p53*, a combination of 2 μg of the *PBase* plasmid (SBI, PB210PA-1) and 6 μg of the overexpressing (or empty *piggyBac* control) plasmid were electroporated into 4×10^6 *p53*-KO haESCs using the same electroporating conditions described above. After transfection for 4–5 days, GFP and haploidy double-positive cells were sorted for subsequent experiments. Overexpression of *Cdk2* and *MAPK11* plasmids and *PBase* plasmid were transfected into WT-haESCs, respectively. After transfection for 4–5 days, GFP and haploidy double-positive cells were sorted for subsequent experiments. To obtain GFP-labeling cell lines, we electroporated a combination of 2 μg of the *PBase* plasmid (SBI, PB210PA-1) and 6 μg of the *piggyBac*-GFP plasmid into 4×10^6 *p53*-KO haESCs, *p53*-KO diESCs, or WT-haESCs, independently.

Differentiation of *p53*-KO haESCs

To detect the DNA contents of haploid embryonic bodies (haEBs) derived from *p53*-KO haESCs, we cultured the cells with Ndiff medium (Takara, Y40002) in noncoated Petri dishes (Falcon) for 7 days. EB aggregates were then dissociated with 0.05% trypsin/EDTA (Gibco, 25300062), and the DNA content was analyzed by FACS. To generate haEpiLCs, we added *p53* KO-1 cells to the wells of a 12-well plate coated with human fibronectin (Yeasen, 40105ES08) in EpiSC medium (Ndiff medium [Takara, Y40002] containing 20 ng/mL activin A [PeproTech, 120-14E-100] and 12 ng/mL bFGF [PeproTech, AF-100-18B-100]). The medium was changed every day, and standard EpiLC colonies emerged 2–3 days later. Fully grown haEpiLCs were passaged with 0.05% trypsin/EDTA and further cultured in EpiSC medium. After sorting for haploid cells 2–3 times (around 14 days), DNA content of haEpiSCs was analyzed. To generate haNSCLCs, we first established a *Pax6*-GFP *p53* KO-1 cell line as described previously (Li et al., 2018b). Four-day EB aggregates derived from *Pax6*-GFP *p53* KO-1 cells were then plated in fibronectin-precoated Petri dishes. After 9 days, *Pax6*-GFP-positive cells were sorted. The DNA content of the *Pax6*-GFP-positive/negative cells was then analyzed. Sorted *Pax6*-GFP-positive haploid cells were further cultured in N2B27 medium supplemented with 10 ng/mL EGF (PeproTech, AF-315-09-100) and 10 ng/mL bFGF (PeproTech, AF-100-18B-100) for proliferation.

For neuronal differentiation, haNSCLCs were plated into dishes precoated with poly-D-lysine (Sigma, P4957) and laminin (Sigma, L2020) and cultured in N2B27 medium supplemented with 20 ng/mL brain-derived neurotrophic factor (PeproTech, AF-450-02) and 20 ng/mL neurotrophin-3 (PeproTech, AF-450-03) to generate neurons. After 2 weeks, the differentiated haNSCLCs were examined for the expression of neuronal (TUJ1, MAP2, and NEUN) and oligodendroglial (O4) markers. For astrocyte differentiation, haNSCLCs were exposed to 1% fetal bovine serum and 10 ng/mL bone morphogenetic protein 4 (PeproTech, AF-120-05ET) in N2B27 medium for 5 days, followed by GFAP staining.

Chimeric Assay and Teratoma Formation

E6.5, E8.5, and E10.5 chimeric embryos were generated by injecting GFP-labeling *p53*-KO haESCs, *p53*-KO diploid ESCs, or WT-haESCs cells into CD-1 background blastocysts. Reconstructed embryos were transferred to the oviducts of pseudopregnant CD-1 mice at 0.5 dpc. At E6.5, E8.5, and E10.5, pseudopregnant mice were sacrificed to dissect chimeric fetuses. Chimeric embryos were trypsinized and GFP-positive and DNA-content analysis performed by FACS.

For teratoma analysis, approximately 1×10^7 *p53* KO-1 cells were injected subcutaneously into the limbs of 8-week-old male SCID mice. Fully formed teratomas were dissected 3 weeks later, then fixed in 4% paraformaldehyde, embedded in paraffin, sectioned, and stained with H&E for further analysis. Alternatively, fully formed teratomas were dissected to analyze the DNA contents.

Data and Code Availability

The Gene Expression Omnibus accession number for the RNA-seq data reported in this paper is GEO: GSE148118.

A complete description of the methods can be found in Supplemental Information.

SUPPLEMENTAL INFORMATION

Supplemental Information can be found online at https://doi.org/10.1016/j.stemcr.2020.05.004.

REFERENCES

Aladjem, M.I., Spike, B.T., Rodewald, L.W., Hope, T.J., Klemm, M., Jaenisch, R., and Wahl, G.M. (1998). ES cells do not activate p53-dependent stress responses and undergo p53-independent apoptosis in response to DNA damage. Curr. Biol. *8*, 145–155.

Betschinger, J., Nichols, J., Dietmann, S., Corrin, P.D., Paddison, P.J., and Smith, A. (2013). Exit from pluripotency is gated by intracellular redistribution of the bHLH transcription factor Tfe3. Cell *153*, 335–347.

Carette, J.E., Guimaraes, C.P., Varadarajan, M., Park, A.S., Wuethrich, I., Godarova, A., Kotecki, M., Cochran, B.H., Spooner, E., Ploegh, H.L., et al. (2009). Haploid genetic screens in human cells identify host factors used by pathogens. Science *326*, 1231–1235.

Cross, S.M., Sanchez, C.A., Morgan, C.A., Schimke, M.K., Ramel, S., Idzerda, R.L., Raskind, W.H., and Reid, B.J. (1995). A p53-dependent mouse spindle checkpoint. Science *267*, 1353–1356.

de Godoy, L.M., Olsen, J.V., Cox, J., Nielsen, M.L., Hubner, N.C., Frohlich, F., Walther, T.C., and Mann, M. (2008). Comprehensive mass-spectrometry-based proteome quantification of haploid versus diploid yeast. Nature *455*, 1251–1254.

Elling, U., Taubenschmid, J., Wirnsberger, G., O'Malley, R., Demers, S.P., Vanhaelen, Q., Shukalyuk, A.I., Schmauss, G., Schramek, D., Schnuetgen, F., et al. (2011). Forward and reverse genetics through derivation of haploid mouse embryonic stem cells. Cell Stem Cell *9*, 563–574.

Freimann, R., and Wutz, A. (2017). A fast and efficient size separation method for haploid embryonic stem cells. Biomicrofluidics *11*, 054117.

Fujiwara, T., Bandi, M., Nitta, M., Ivanova, E.V., Bronson, R.T., and Pellman, D. (2005). Cytokinesis failure generating tetraploids promotes tumorigenesis in p53-null cells. Nature *437*, 1043–1047.

Gibbons, B., MacCallum, P., Watts, E., Rohatiner, A.Z., Webb, D., Katz, F.E., Secker-Walker, L.M., Temperley, I.J., Harrison, C.J., Campbell, R.H., et al. (1991). Near haploid acute lymphoblastic leukemia: seven new cases and a review of the literature. Leukemia *5*, 738–743.

Guo, A., Huang, S., Yu, J., Wang, H., Li, H., Pei, G., and Shen, L. (2017). Single-cell dynamic analysis of mitosis in haploid embryonic stem cells shows the prolonged metaphase and its association with self-diploidization. Stem Cell Reports *8*, 1124–1134.

Hafner, A., Bulyk, M.L., Jambhekar, A., and Lahav, G. (2019). The multiple mechanisms that regulate p53 activity and cell fate. Nat. Rev. Mol. Cell Biol. *20*, 199–210.

He, Z.Q., Xia, B.L., Wang, Y.K., Li, J., Feng, G.H., Zhang, L.L., Li, Y.H., Wan, H.F., Li, T.D., Xu, K., et al. (2017). Generation of mouse haploid somatic cells by small molecules for genome-wide genetic screening. Cell Rep. *20*, 2227–2237.

He, W., Zhang, X., Zhang, Y., Zheng, W., Xiong, Z., Hu, X., Wang, M., Zhang, L., Zhao, K., Qiao, Z., et al. (2018). Reduced self-diploidization and improved survival of semi-cloned mice produced from androgenetic haploid embryonic stem cells through overexpression of Dnmt3b. Stem Cell Reports *10*, 477–493.

Kondrashov, A.S., and Crow, J.F. (1991). Haploidy or diploidy: which is better? Nature *351*, 314–315.

Leeb, M., and Wutz, A. (2011). Derivation of haploid embryonic stem cells from mouse embryos. Nature *479*, 131–134.

Leeb, M., Walker, R., Mansfield, B., Nichols, J., Smith, A., and Wutz, A. (2012). Germline potential of parthenogenetic haploid mouse embryonic stem cells. Development *139*, 3301–3305.

Leeb, M., Dietmann, S., Paramor, M., Niwa, H., and Smith, A. (2014). Genetic exploration of the exit from self-renewal using haploid embryonic stem cells. Cell Stem Cell *14*, 385–393.

Li, Y., and Shuai, L. (2017). A versatile genetic tool: haploid cells. Stem Cell Res. Ther. *8*, 197.

Li, M., Yu, J.S.L., Tilgner, K., Ong, S.H., Koike-Yusa, H., and Yusa, K. (2018a). Genome-wide CRISPR-KO screen uncovers mTORC1-mediated Gsk3 regulation in naive pluripotency maintenance and dissolution. Cell Rep. *24*, 489–502.

Li, Y., Li, X., Wang, H., Gao, Q., Zhang, J., Zhang, W., Zhang, Z., Li, L., Yu, Y., and Shuai, L. (2018b). CRISPR/Cas9-edited Pax6-GFP reporter system facilitates the generation of mouse neural progenitor cells during differentiation. J. Genet. Genomics *45*, 277–280.

Lin, T., Chao, C., Saito, S., Mazur, S.J., Murphy, M.E., Appella, E., and Xu, Y. (2005). p53 induces differentiation of mouse embryonic stem cells by suppressing Nanog expression. Nat. Cell Biol. *7*, 165–171.

Melino, G., De Laurenzi, V., and Vousden, K.H. (2002). p73: friend or foe in tumorigenesis. Nat. Rev. Cancer *2*, 605–615.

Monfort, A., Di Minin, G., Postlmayr, A., Freimann, R., Arieti, F., Thore, S., and Wutz, A. (2015). Identification of spen as a crucial factor for Xist function through forward genetic screening in haploid embryonic stem cells. Cell Rep. *12*, 554–561.

Olbrich, T., Mayor-Ruiz, C., Vega-Sendino, M., Gomez, C., Ortega, S., Ruiz, S., and Fernandez-Capetillo, O. (2017). A p53-dependent response limits the viability of mammalian haploid cells. Proc. Natl. Acad. Sci. U S A *114*, 9367–9372.

Peng, K., Li, X., Wu, C., Wang, Y., Yu, J., Zhang, J., Gao, Q., Zhang, W., Zhang, Q., Fan, Y., et al. (2019). Derivation of haploid trophoblast stem cells via conversion in vitro. iScience *11*, 508–518.

Perrot, V., Richerd, S., and Valero, M. (1991). Transition from haploidy to diploidy. Nature *351*, 315–317.

Qu, C., Yan, M., Yang, S., Wang, L., Yin, Q., Liu, Y., Chen, Y., and Li, J. (2018). Haploid embryonic stem cells can be enriched and maintained by simple filtration. J. Biol. Chem. *293*, 5230–5235.

Sagi, I., Chia, G., Golan-Lev, T., Peretz, M., Weissbein, U., Sui, L., Sauer, M.V., Yanuka, O., Egli, D., and Benvenisty, N. (2016). Derivation and differentiation of haploid human embryonic stem cells. Nature *532*, 107–111.

Shuai, L., and Zhou, Q. (2014). Haploid embryonic stem cells serve as a new tool for mammalian genetic study. Stem Cell Res. Ther. *5*, 20.

Shuai, L., Li, W., Wan, H., Zhao, X.Y., Wang, L., and Zhou, Q. (2014). Generation of Mammalian offspring by haploid embryonic stem cells microinjection. Curr. Protoc. Stem Cell Biol. *31*, 1A 6 1–15.

Shuai, L., Wang, Y., Dong, M., Wang, X., Sang, L., Wang, M., Wan, H., Luo, G., Gu, T., Yuan, Y., et al. (2015). Durable pluripotency and

haploidy in epiblast stem cells derived from haploid embryonic stem cells in vitro. J. Mol. Cell Biol. *7*, 326–337.

Song, J., Li, J., Hou, F., Wang, X., and Liu, B. (2015). Mangiferin inhibits endoplasmic reticulum stress-associated thioredoxin-interacting protein/NLRP3 inflammasome activation with regulation of AMPK in endothelial cells. Metab. Clin. Exp. *64*, 428–437.

Stiewe, T. (2007). The p53 family in differentiation and tumorigenesis. Nat. Rev. Cancer *7*, 165–168.

Takahashi, S., Lee, J., Kohda, T., Matsuzawa, A., Kawasumi, M., Kanai-Azuma, M., Kaneko-Ishino, T., and Ishino, F. (2014). Induction of the G2/M transition stabilizes haploid embryonic stem cells. Development *141*, 3842–3847.

Wang, H., Zhang, W., Yu, J., Wu, C., Gao, Q., Li, X., Li, Y., Zhang, J., Tian, Y., Tan, T., et al. (2018). Genetic screening and multipotency

in rhesus monkey haploid neural progenitor cells. Development *145*, dev160531.

Xu, H., Yue, C., Zhang, T., Li, Y., Guo, A., Liao, J., Pei, G., Li, J., and Jing, N. (2017). Derivation of haploid neurons from mouse androgenetic haploid embryonic stem cells. Neurosci. Bull. *33*, 361–364.

Yang, H., Liu, Z., Ma, Y., Zhong, C., Yin, Q., Zhou, C., Shi, L., Cai, Y., Zhao, H., Wang, H., et al. (2013). Generation of haploid embryonic stem cells from *Macaca fascicularis* monkey parthenotes. Cell Res. *23*, 1187–1200.

Yi, M., Hong, N., and Hong, Y. (2009). Generation of medaka fish haploid embryonic stem cells. Science *326*, 430–433.

Ying, Q.L., Stavridis, M., Griffiths, D., Li, M., and Smith, A. (2003). Conversion of embryonic stem cells into neuroectodermal precursors in adherent monoculture. Nat. Biotechnol. *21*, 183–186.